Senescence of cortical neurons following persistent DNA double-strand breaks induces cerebrovascular lesions

Caroline A. Kopsidas[1¥], Clara C. Lowe[1¥ ≠], Jun Zhang[1¥], Wenjun Kang[2], Xiaoming Zhou[3], and Yuanyi Feng[1*]

1. Department of Biochemistry and Molecular Biology, Uniformed Services University, 4301 Jones Bridge Road, Bethesda, MD 20814, U.S.A

2. Center for Research Informatics, University of Chicago, Chicago, IL 60637, U.S.A

3. Department of Medicine, Uniformed Services University, 4301 Jones Bridge Road, Bethesda, MD 20814, U.S.A

¥: These authors contributed equally

≠ current address: Wake Forest University School of Medicine, 475 Vine St, Winston-Salem, NC 27101

*To whom correspondence should be addressed:

Tel: (301) 295-9419

Email: yuanyi.feng@usuhs.edu

Abstract

DNA double strand breaks (DSBs), neuroinflammation, and vascular alterations in the brain are all associated with neurodegenerative disorders. However, it remains unclear how these neuropathological changes relate to each other and act synergistically to promote neurodegeneration. Here we reveal cerebrovascular defects caused by abrogating the BRCA1-assocaited protein Brap in cerebral cortical neurons in mice. Brap loss of function results in persistent DSBs and a senescence state in cortical neurons. In this state, upregulation of genes involving in cell secretion as well as encoding inflammatory and vasoactive factors leads to both ischemic and hemorrhagic damages to cerebral blood vessels. The vascular lesions intertwine with neuroinflammation and neuronal DSBs. They impair glycolytic metabolism, increase oxidative stress, and exacerbate neuronal DSBs, resulting in downregulation of genes essential for neuronal function. By demonstrating the non-cell-autonomous cerebrovascular impact of damaged neurons, our data suggest that DSBs can initiate brain-wide neurodegeneration through senescence-mediated secretion.

Introduction

Genome instability with increased DNA double strand breaks (DSBs) is detrimental to neurons of the brain and has been implicated in diverse neurodegenerative disorders (NDs)[1-6]. However, the etiology of NDs is multifaceted, the progressive decline in number and activity of neurons exhibits significant comorbidity with glial and cerebrovascular abnormalities[7-10]. Thus, determining the mechanism by which neuronal DSBs interact with glial and vascular dysfunction in the brain is essential for understanding the pathophysiology that underlies brain-tissue-wide degeneration.

By studying chromatin remodeling in neurogenesis, we have recently shown that DSBs in neocortical neurons may arise from compromised epigenetic silencing of pericentric satellite DNA in mice with genetic deficiencies of Nde1 (neurodevelopment protein 1) and its interacting Brap (BRCA1-associated protein)[11]. The long tandem repeats of satellite DNA are intrinsically unstable and refractory to repair[12]. We found that the de-repression of satellite repeats in Brap neural progenitor cell (NPC) or neuronal conditional knockout (cKO) mice ($Brap^{cKONPC}$ and $Brap^{cKONeuron}$, respectively) results in persistent DSBs in cortical neurons and subsequently a senescence state along with accelerated neurodegeneration and shortened lifespan[13]. In vivo, cellular senescence is characterized by the distinctive senescence associated secretory phenotype (SASP)[14-20], through which it imposes micro-environmental effects to the nearby tissue. By secreting a complex mixture of pro-inflammatory and pro-oxidative cytokines, chemokines, growth factors, and proteases, SASP can induce inflammation and aging[21-26]. Indeed, cellular senescence in cerebral cortices of $Brap^{cKONPC}$ mice was accompanied by the upregulation of secreted molecules involving not only immune regulation but also neural networking and

cerebrovascular activities[13], which suggests that senescence is a mediator by which neurons with DSBs impair their neighboring cells in the surrounding brain tissue.

In this report, we provide proof of concept evidence on the non-cell-autonomously effect of neuronal DSBs through studying pathological consequences of mice in which Brap is abrogated in various cell types of the brain. We present the finding that Brap loss of function (LOF) in cortical excitatory neurons can cause diverse cerebrovascular lesions. These vascular damages co-occur with neuroinflammation and synergize with DSBs, resulting in brain metabolic and redox dysfunction to accelerate neurodegeneration. These results suggest that SASP is a mechanism through which genotoxic insults, especially DSBs in repetitive sequences of cortical neurons, impinge on broad brain regions.

Results

Brap abrogation in cortical neurons causes diverse cerebrovascular lesions

While Brap LOF results in DSBs and cellular senescence of replication competent cells in culture, DSBs in the cerebral cortex were detected only in neurons of mice in which Brap was abrogated by Emx1-Cre in NPCs that give rise to cortical glutamatergic neurons, astroglia, and oligodendrocytes[27] or by Thy1-Cre in postnatal cortical and hippocampal neurons[28] (referred to as $Brap^{cKONPC}$ and $Brap^{cKONeuron}$, respectively, or collectively as neural $Brap^{cKO}$ mice hereafter unless noted specifically)[13]. These mutant mice show rapid brain degeneration and premature death starting at the young adult age (Fig. 1A). To understand the cause of mortality and neurodegeneration, we monitored neural $Brap^{cKO}$ mice closely and found death in more than half of them occurred suddenly without any sign of fatal conditions the day before, though the mutant mice were overtly hyperactive and some showed transient episodes of seizures (Supplemental

videos 1 and 2). We were able to catch about 40 male and female neural Brap^{cKO} mice that showed sudden onset of fatal symptoms, including extreme lethargy, labored breathing, or hemi/monoplegia, which suggested death was imminent (Fig. 1B, Supplemental videos 3 and 4). On examination, about 20% of them showed visible subarachnoid and/or intracerebral hemorrhage (Fig. 1C). Histological and immunohistological analyses of these mutant brains revealed widespread cerebrovascular lesions (Fig. 1D, E). While some intracerebral blood vessels appeared leaky with albumin extravasation, it frequently co-occurred with occlusions in cerebral vessels in these mutant mice. These data suggest that the sudden death of neural Brap^{cKO} mice was due to both ischemic and hemorrhagic damages of cerebral blood vessels.

To verify the co-occurrence of cerebrovascular obstruction and bleeding, we examined over 50 neural Brap^{cKO} mice between weaning and 12 months of age. We found cerebral vessels in about ~60% of the mutant mice had occlusions enriched with Cd42b, a marker for platelet activation and clot formation (Fig. 1F). The presence of cerebrovascular clots and thrombosis was further confirmed by high levels of D-dimer, the product of fibrin degradation (Fig. 1G). In addition to blocked vessels, cerebral aneurysm, defined by isolated blood vessel dilation, balloons, or bulges, was also shown by about 20% of the neural Brap^{cKO} mice (Fig. 1D, H). These vascular lesions affected predominantly cerebral vessels of < 100um in diameter, distributed sporadically throughout the cerebrum in the subarachnoid space, the neocortex, the white matter, and sometimes in other brain regions (Fig. 1D-H, Fig. S1A). The cerebral vascular defects were comparable in Brap^{cKONPC} and Brap^{cKONeuron} mice but were not shown by their control counterparts (Brap$^{flox/wt}$; Cre-), which suggests that Brap LOF in the cortical parenchyma, can cause diverse secondary damages in cerebral small vessels.

To ascertain that the cerebrovascular defects were caused by Brap LOF in neurons, we generated and analyzed mice in which Brap was deleted in excitatory neurons of the forebrain and the CA1 of hippocampus by Camk2a-Cre[29] ($Brap^{cKOENeuron}$) and vascular endothelial cells by Tek-Cre[30] ($Brap^{cKOEC}$), respectively. In contrast to the mild survival impairment and subtle brain pathological detects of $Brap^{cKOEC}$ mice (Fig. 1A, Fig. S1B), $Brap^{cKOENeuron}$ mice, in which Brap was broadly abrogated in excitatory neurons of the neocortex, hippocampus, striatum, and other brain structures, showed not only vascular defects but also a stronger survival disadvantage than $Brap^{cKONPC}$ and $Brap^{cKONeuron}$ mice (Fig 1A,C; Fig. S1B). Therefore, the shared phenotype of mice with loss of Brap commonly in cortical excitatory neurons provides compelling evidence for a non-autonomous cerebrovascular impact of cortical excitatory neuronal defects. This finding fully agrees with the notion that Brap deficient cortical excitatory neurons with persistent DSBs can enter a senescence state and affect vascular cells in their nearby cortical tissue.

Co-upregulation of coagulation, hypoxia, inflammatory, and DNA damage responses

To determine the molecular profile by which neuronal Brap LOF affects the cerebral vasculature, we performed transcriptome analysis of $Brap^{cKONPC}$, $Brap^{cKONeuron}$, and $Brap^{cKOEC}$ mice at 3-4 months of age along with age matched control mice ($Brap^{flox/wt;}$ Cre-). We analyzed poly(A) enriched cortical mRNA and obtained more reads than the previous RNAseq of total cortical RNA from $Brap^{cKONPC}$ mice[13]. Compared with control mice, $Brap^{cKONPC}$ and $Brap^{cKONeuron}$ mice showed a total of 3301 and 1962 differentially expressed genes (DEGs; FDR<0.05; Fold Change >1.5), respectively, whereas $Brap^{cKOEC}$ mice only showed 13 DEGs (Fig. 2A). Gene ontology (GO) analyses revealed that the 1570 and 1205 significantly upregulated DEGs in $Brap^{cKONPC}$ and $Brap^{cKONeuron}$ mice, respectively, were enriched most significantly in cellular components

associated with secretory pathways, including cytoplasmic vesicles, extracellular exosomes and vesicles, secretory granules and vesicles, as well as the cell substrate junction (Fig. 2B). Such substantial increase in the expression of genes involving cell secretion strongly supports the non-cell autonomous effects of Brap deficient neurons via SASP.

We next performed gene set enrichment analysis (GSEA) to compare the transcriptome of $Brap^{cKONPC}$ or $Brap^{cKONeuron}$ mice relative to their control counterparts. These two datasets demonstrated the phenocopy of Brap LOF in cortical NPCs and neurons with respect to significant enrichments for genes implicated in over 20 hallmark pathways, including inflammation response, TNFα signaling via NFkB, interferon-γ response, coagulation, hypoxia, ROS pathway, P53 pathway, and DNA repair (Fig. 2C, Table S1). Likewise, GO analyses of significantly upregulated DEGs in $Brap^{cKONPC}$, and $Brap^{cKONeuron}$ cortices revealed strong enrichments of genes associated with biological processes in inflammatory and vascular responses to stimuli, wound, and oxygen-containing compounds (Fig. 2D). Collectively, the transcriptomic data suggest that, in spite of the elevation of DNA repair, DSBs in Brap deficient cortical neurons persist and drive them to an irreversible senescent state, under which a large number of inflammatory and vascular regulatory genes are upregulated, leading to multiple secondary effects on local astroglia, microglia, and blood vessels.

We confirmed the elevation of selected vasoactive molecules in neural $Brap^{cKO}$ mice by RT-qPCR. These include Pai1(Serpine1), a bona fide SASP molecule that inhibits tissue plasminogen activator (tPA) and blocks clot breakdown[31-33], α2-antiplasmin (Serpinf2), a potent plasmin inhibitor that stops fibrinolysis[34-36], Vwf, a key player in thrombus formation by facilitate platelet adhesion to damaged vascular walls[37], Adm (Adrenomedullin), a vasodilator peptide[38,39], Mmp9, a matrix metalloprotease that acts on the vascular wall[40-42], Agt

(Angiotensinogen), the precursor for all angiotensin peptides that promote vasoconstriction and blood pressure increase[43], Avp (Vasopressin), a peptide hormone that constricts arterioles and raises blood pressure[44,45], and Edn1 (endothelin-1), a strong and long-acting vasoconstrictive peptide that can induce stroke[46-48](Fig. 2E). These factors can act differentially and/or synergistically to induce heterogeneous vascular changes. Their significant upregulation in the cortical tissue indicates the loss of neurovascular hemostasis, which explains the diverse ischemic and hemorrhagic defects in cerebral small vessels and the sudden midlife mortality of neural Brap^{cKO} mice.

All neural Brap^{cKO} mice with significant upregulation of vasoactive molecules also showed increased expression of genes associated with neuroinflammation and microglia activation, such as CD68, Tnfα, Il6, Ccl2, Cxcl10, and Icam1 (Fig. 2F). As inflammation is a major hallmark of cellular senescence, these data demonstrate a SASP-mediated dual-effect of intractable neuronal DSBs on cortical inflammatory and vascular cells.

Intermingle of cerebrovascular lesions with neuroinflammation and neuronal DSBs

To further reveal the paracrine effect of neuronal senescence, we performed immunohistological analyses to access the spatial correlation of cerebral vascular lesions with inflammatory responses of glial cells and neuronal DSBs in neural Brap^{cKO} mice. While astrogliosis and microgliosis are highly elevated in Brap^{cKONPC} and Brap^{cKONeuron} cortices[13], we found the activated astrocytes and microglia were closely associated with vascular lesions. We detected reactive astrocytes by Gfap immunoreactivity and active microglia by their retracted ramification and enlarged roundish soma with Iba immunostain, and found they were highly abundant in the vicinity of occluded, bulged, or ruptured cerebral blood vessels in neural Brap^{cKO} mice (Fig. 3A-

D; Fig. S2A-C). Furthermore, we show that damaged and misshapen cerebral vessels were also surrounded by neurons with high levels of γH2A.X, a biomarker for DSBs (Fig 3E, F; Fig. S2D). Although vascular injury can trigger gliosis, and conversely, neuroinflammation may augment vascular defects, their co-occurrence with neurons showing high levels of DSBs suggests they were both initiated by neuronal senescence.

We also detected structural defects in cerebral blood vessels of neural $Brap^{cKO}$ mice. Damaged vascular wall, evidenced by loss of smooth muscle actin, was shown by those cerebral vessels with occlusions, aneurysm or rupture in the acute stage of vascular lesions of the mutant mice (Fig. 3G, Fig. S2E). Cerebral edema with vacuolar appearance of the gray matter and enlargement of perivascular space, which are common signs of intracerebral small vessels defects, were presented by neural $Brap^{cKO}$ brains (Fig. 3H). Furthermore, we detected a significant increase in blood brain barrier (BBB) permeability in presymptomatic $Brap^{cKONPC}$ mice (Fig. 3I). In those $Brap^{cKONPC}$ mice that survived past 6 months, there were elevations of collagen deposition and loss of elastin in cerebral blood vessels (Fig. 3J,K), which are signs of basement membrane thickening and increased vascular stiffness. These vascular changes suggest chronic cerebral hypoperfusion in the surviving neural $Brap^{cKO}$ mice.

Compromised glycolysis, increased ROS, neuronal necrosis, and down-regulation of genes essential for neuron function

We next sought to determine the impact of vascular lesions on brain metabolism and neural function in neural $Brap^{cKO}$ mice. The brain relies on uninterrupted supply of glucose and oxygen from blood flow to support neuronal activities. Glucose is the primary fuel and mainly metabolized through glycolysis to first generate pyruvate while turning NAD^+ (nicotinamide

adenine dinucleotide) to its reduced form, NADH. In the presence of oxygen, pyruvate is further processed by the mitochondrial Krebs cycle during which more NADH is generated to donate electrons in the respiratory chain for ATP synthesis. Alternatively, glucose can enter the pentose phosphate pathway (PPP), producing NADPH (reduced form of nicotinamide adenine dinucleotide phosphate, $NADP^+$) to support diverse biosynthesis and scavenge reactive oxygen species (ROS). We thus assessed the levels of NADH, NADPH, and ROS to determine the metabolic flux and redox status. We found that the level of NADH was significantly lower in the cortical tissue of neural $Brap^{cKO}$ than in that of control mice (Fig. 4A), which is consistent with reduced glycolytic flux due to glucose and oxygen deprivation resulting from blocked blood flow. Parallel to decreased NADH, neural $Brap^{cKO}$ cortices showed significantly increased NADPH and ROS (Fig. 4B, C), which suggest a glucose metabolic switch from glycolysis to PPP towards ROS detoxification. In line with this, we observed cells with strong endogenous fluorescence in freshly prepared cortical sections of neural $Brap^{cKO}$ mice (Fig. 4D-F). Such fluorescence signals were detected specifically by the microscopic green fluorescence channel, which match the emission peak of 440-470 nm of NADH or NADPH's autofluorescence[49]. We further found that cells with green autofluorescence were largely segregated from sites of microbleeds where the autofluorescence of red blood cells and hemoglobin was shown in both green and red channels (Fig. 4E). These green auto-fluorescent cells were predominantly excitatory neurons, as evidenced by their pyramidal morphology, positive for the pan-neuronal marker NeuN, and rare expression of GABAergic neuronal marker parvalbumin (Fig. 4F, Fig. S3A). Given that the significant elevation of NADPH in neural $Brap^{cKO}$ cortical tissues was coupled with increased ROS and decreased NADH, the green autofluorescence reflects the attempt made by excitatory neurons to increase NADPH and fight against oxidative stress.

Despite the upregulation of NADPH, neural Brap^{cKO} cortices showed significant upregulation of genes associated with cell death and apoptosis (Fig. 4G,H), suggesting a dominant impact of metabolic dysfunction on neuronal survival. Although we did not detect apoptotic cells in neural Brap^{cKO} brains by cleaved caspase 3 immunoreactivity, decreases in neuronal density were evident in areas with active microbleeding (Fig. S3B). We observed "red neurons" in the cerebral cortex of neural Brap^{cKO} mice (Fig. 4I). These acidophilic neurons presented deep red eosinophilic cytoplasm, cell body shrinkage, and pyknotic nuclei, which are characteristic for neuronal damages resulting from hypoxic ischemic brain injuries and usually lead to necrotic neuronal death[50]. We also observed band-like lesions with enrichment of condensed nuclei in neocortical layer III of neural Brap^{cKO} mice (Fig. 4J), which was reminiscent of the pseudo-laminar necrosis resulting from the glucose and oxygen deficiency of cerebral hypoxic-ischemic insults[51]. Notably, high levels of DSBs were also prevalent in these layer III neurons of the neural Brap^{ckO} mice (Fig. 4K, Fig. S3C). This suggests the association of selective vulnerability to metabolic stress with DSBs, the feed-forward contribution of vascular defects to neuronal genome instability, and the synergy of genotoxicity and vascular damage in impairing neuronal function and survival.

We further looked into transcripts downregulated in neural Brap^{cKO} cortices to assess neuronal dysfunctions associated with compromised glycolysis and increased oxidative stress. Compared with control mice, 1731 and 757 genes showed significantly decreased expression in cortical tissues of Brap^{cKONPC} and Brap^{cKONeuron} mice, respectively. GO enrichment analyses revealed that these drown-regulated genes are most significantly enriched in those cellular components specifically essential for neurons, such as neuronal projections, dendrites, synapses, and ion channel complexes (Fig. 4L). They mainly encode molecules with functions in ion

channel activities, metal ion transports, and Ca^{2+} signaling (Fig. 4M); they predominantly engage in biological processes in neuron differentiation, morphogenesis, synaptic signaling, and synaptic transmission (Fig. 4N). These data are consistent with the rapid neuronal function decline of neural $Brap^{cKO}$ mice and strongly support the contribution of vascular and metabolic dysfunction to their accelerated neurodegeneration.

Discussion

Our analysis uncovered a non-cell autonomous effect of neuronal DSBs on cortical glia and vasculature. This finding provides an insight into the synergistic contribution of multiple risk factors for neurodegeneration. While NDs are primarily caused by loss of neurons or neuronal function, they are almost inevitably associated with inflammatory responses of astroglia and microglia as well as alterations in cerebral blood vessels[8-10]. In particular, vascular dementia is the second most common cause after Alzheimer's disease (AD) for cognitive impairments[52-54]. As the brain uses 20% of the body's energy to support the constant neuronal activities, it fully relies on uninterrupted blood flow. This requires neurons to make physical and functional interactions with glia and vascular cells, which together form the neurovascular unit (NVU)[55,56]. Therefore, defects in any constituents of the NVU is expected to result in co-occurrence of neuroinflammation, vascular changes, and neuronal dysfunction. Both cerebral vascular diseases and NDs have a wide range of clinical manifestation and can go silently for decades before causing stroke and dementia at old age. Results of this study highlight an unexpected mechanism connecting neuronal damages with cerebrovascular lesions. The robust cerebral vascular and neurodegenerative phenotype of the neural $Brap^{cKO}$ mouse model also shows a very early onset.

It may serve as a new tool for further investigating the etiology, diagnosis, and intervention of both vascular and neurodegenerative dementia.

The main fate of cells with Brap LOF is cellular senescence, driven primarily by recurrent DSBs due to insufficient silencing of satellite repeats[11,13]. The senescence state permits a direct communication of neurons with their supporting cells. Cellular senescence, though was originally discovered as the state of irreversible cell cycle arrest in culture, presents much more complex phenotypes in vivo. It is a highly dynamic state and can influence multiple other cells with the paracrine effect of SASP. The molecular composition of SASP is context dependent, with which senescent cells can drive normal cells in their neighbor into secondary senescence[57]. We detected the upregulation of a large number of secreted molecules in the cortical tissue of neural $Brap^{cKO}$ mice. Although neuronal DSBs and senescence may primarily account for these molecular changes, secondary senescence of glia and vascular cells or their reaction to senescent neurons likely contribute significantly to the diverse inflammatory and vasoactive molecules underpin the vascular lesions, neurodegeneration, and mortality of neural $Brap^{cKO}$ mice. Thus, senescence may act not only as a cell autonomous defense response but also a mechanism for promoting synergistic actions in cells of NVU.

Results of this study also reveal a dominant role of neurons and their defects in influencing cerebral vasculature and driving systemic brain degeneration. Although the molecular exchange between neurons and cerebral blood circulation is highly restricted by the blood brain barrier/BBB, BBB's permeability may be increased by SASP-mediated local increase in proteases and inflammatory factors. This suggests a contribution of neuronal senescence to BBB breakdown in AD and other NDs[10]. Senescence in vivo encompasses cells in heterogeneous states. Besides the association with age-related pathologies, senescence can also

be a beneficial process in embryogenesis, wound healing, tumor suppression, and tissue homeostasis[58-60]. Neurons could be considered "senescent cells" by the canonical definition of "irreversible cell cycle arrest" and by the fact that they harbor a large number of somatic mutations[61]. While this study focuses on the detrimental effect of neuronal DSBs and senescence in inducing cerebrovascular damage, it opens a possibility for future study to test whether SASP-secretion is used as a physiological mechanism for neuronal activity to modulate BBB function and local cerebral blood flow, and whether SASP molecules may serve as therapeutic targets for NDs.

Materials & Methods

Mice

Brap floxed (*Brap*$^{flox/flox}$) mice were generated by conventional mouse embryonic stem cell-based gene targeting[62,63]. Brap^{cKONPC} mice were generated by crossing Brap$^{flox/flox}$ mice with the Emx1-Cre mice purchased from JaxMice (stock # 005628). Brap^{cKONeuron} mice were generated by crossing Brap$^{flox/flox}$ mice with Thy1-cre mice purchased from JaxMice (Stock No: 006143). Brap^{cKOEC} mice were generated by crossing Brap$^{flox/flox}$ mice with the Tek-Cre (Tie2-Cre) mice purchased from JaxMice (stock # 008863). Brap^{cKOENeuron} mice were generated by crossing Brap$^{flox/flox}$ mice with the Camk2a-Cre mice (T29-1) purchased from JaxMice (stock # 005359). All mice used for this study were housed and bred according to the guidelines approved by the IACUC committees of Uniformed Services University of Health Services in compliance with the AAALAC's guidelines. Experiments were performed using littermates or age and genetic background matched control and mutant groups in both sexes.

Fluorescence immunohistological and immunochemical analyses

For immunofluorescence staining of mouse cortical tissue, mouse brains were fixed by transcardial perfusion with PBS and 4% paraformaldehyde and then processed in 12um cryosections or 5 um paraffin sections. After treating with antigen unmasking solutions (Vector Labs), brain sections were blocked with 5% goat serum and incubated with primary antibodies in PBS, 0.05% Triton X100, and 5% goat serum at 4°C overnight, and followed by staining with fluorescence conjugated antibodies and Hoechst 33342. Epifluorescence images were acquired with a Leica CTR 5500 fluorescence, DIC, and phase contrast microscope equipped with the Leica DFC7000T digital camera. For immunohistological (IHC) brain analysis, paraffin sections of 5um thickness were treated with antigen unmasking solutions, blocked with 5% goat serum for one hour, incubated with primary antibodies in PBS, 0.05% Triton X100, and 5% goat serum at 4°C overnight. Then the immunosignals were detected by HRP-conjugated secondary antibodies and the DAB substrate using an ABC kit (Vector lab). IHC images were acquired with a Leica CTR 5500 fluorescence, DIC, and phase contrast microscope equipped a Leica DFC7000 T camera. Images were imported to Adobe Photoshop and adjusted for brightness and black values.

RNA isolation and RT-qPCR

Cerebral cortical tissue was homogenized in TRIzol reagent (Thermo Fisher) followed by total RNA extraction according to the manufacturer's protocol. 1ug RNA was reverse transcribed into first-strand cDNA using Superscript III reverse transcriptase (Invitrogen). RT-qPCR reactions were performed using Power SYBR Green PCR Master Mix on an Applied Biosystems Step One Plus Real-Time PCR Systems. Primers used for accessing gene expression were

synthesized according to validated primer sequences from the MGH-PGA PrimerBank, and are listed in Table S2, RT-qPCR primers. Expression was normalized to TATA-binding protein (Tbp) as an internal control and results were analyzed using the $2^{-(\Delta\Delta CT)}$ method.

Bulk RNA sequencing analysis

Purified total RNA from whole cerebral cortical tissue of four control ($Brap^{flox/wt\ Cre-}$), six $Brap^{cKONPC}$, five $Brap^{cKONeuron}$, and five $Brap^{cKOEC}$ mice at 3 months of age were processed at the University of Chicago Genomics Facility, where Poly-A+ selected RNA libraries were prepared and sequenced using an Illumina HiSeq 4000 platform (100 bp paired-end reads). RNA sequencing files were transferred to the Tarbell High-performance computing cluster of Center for Research Informatics at the University of Chicago for analysis.

The quality of raw sequencing data was assessed using FastQC v0.11.5. Raw reads were mapped to the mouse reference transcriptome (GRCm38) using Salmon version 1.5.2. After read mapping with Salmon, Bioconductor (https://bioconductor.org/packages/release/bioc/html/tximport.html) was used to read Salmon outputs into the R environment. Annotation data from Gencode vM25 was used to summarize data from transcript-level to gene-level. Filtering was carried out to remove non protein coding or lowly expressed genes. We first removed the non-protein coding genes, which reduced the number of genes from 54418 to 21828. Then genes with less than 1 count per million (CPM) in at least 3 or more samples were filtered out, which reduced the number of genes from 21828 to 14086. A variety of R packages was used for data analysis. All graphics and data wrangling were handled using the tidyverse suite of packages. All packages used are available from the Comprehensive R Archive Network (CRAN), Bioconductor.org, or Github. Differential gene

expression analysis was performed using the DESeq2 package. Significance was defined as FDR <0.05 and absolute Fold Change ≥ 1.5.

Brain metabolic analyses

To assess the glycolic flux and redox status, cortical tissues were dissected from mice that were deeply anesthetized and euthanized by cervical dislocation. The tissue specimens were minced on ice, aliquoted, and stored at -80°C for metabolic analysis. The NADH/NAD+ assay was performed using NAD/NADH Quantitation Colorimetric Kit (BioVision) according to manufacturer's protocol. The NADPH/NADP+ assay was performed using NADP/NADPH Quantitation Kit (Sigma-Aldrich) according to manufacturer's protocol. The level of ROS was detected by the OxiSelect™ Green Fluorescence In Vitro ROS/RNS Assay Kit (CELL BIOLABS) according to manufacturer's protocol. Quantities of cortical proteins were determined by Pierce™ Detergent Compatible Bradford Assay Kit (Thermo Scientific™).

Evans blue assay

Mice were given an intraperitoneal injection of 2% Evans blue solution (Sigma E2129, dissolved in PBS and filtered through a 0.22um filer, at 4 ml/kg of body weight). The dye was allowed to circulate for 4 hours. Then mice were perfused with 60 ml ice-cold PBS to clear the Evans blue in circulation and euthanized by cervical dislocation. Cerebral cortices were dissected, flash frozen in liquid nitrogen, wrapped in aluminum foil and stored at −80°C. To quantify the amount of Evans blue in cortical tissues, samples were dried in an oven at 55°C, weighted, and immersed in formamide to extract Evans blue from the tissue. After removing tissue precipitates by centrifugation, the amount of Evans blue in the supernatant was determined by absorbance at a

wavelength of 620 nm and quantified according to a standard curve. Results were presented as OD 620 per gram of dry cortical tissue.

Quantification and statistical analysis

No statistical methods were used to predetermine sample size, while all experiments were performed with a minimum of three biological replicates and all cell counts were obtained from at least ten random fields. The experiments were not randomized; the investigators were not blinded to the sample allocation and data acquisition during experiments but were blinded in performing quantitative analyses of immunohistological images using the NIH Image J software. All statistical analyses were done using GraphPad Prism 9.0 software. Data were analyzed by one-way ANOVA or unpaired two-tailed Student's t tests for comparing differences between different genotypes. Differences were considered significant with a p value < 0.05.

Acknowledgments

The authors wish to thank the Genomics Facility of University of Chicago for RNA library construction and NGS analysis. This work was supported by startup funds of Uniformed Services University of the Health Sciences to Y.F.

Author contributions

Y.F. conceptualized the project, designed and performed the experiments, interpreted the results, and wrote the manuscript. C.A.K. performed experiments; C.C.L. initiated the study and performed the experiments; J. Z. performed experiments; W.K. performed data analyses, X.Z. assisted with experiments.

Competing interests

The authors declare that they have no conflict of interest.

Disclaimer

The opinions, interpretations, conclusions and recommendation are those of the authors and are not necessarily endorsed by the U.S. Army, Department of Defense, the U.S. Government or the Uniformed Services University of the Health Sciences. The use of trade names does not constitute an official endorsement or approval of the use of reagents or commercial hardware or software. This document may not be cited for purposes of advertisement.

References

1. Shanbhag, N.M., *et al.* Early neuronal accumulation of DNA double strand breaks in Alzheimer's disease. *Acta Neuropathol Commun* **7**, 77 (2019).
2. Welch, G.M., *et al.* Neurons burdened by DNA double-strand breaks incite microglia activation through antiviral-like signaling in neurodegeneration. *Sci Adv* **8**, eabo4662 (2022).
3. Suberbielle, E., *et al.* Physiologic brain activity causes DNA double-strand breaks in neurons, with exacerbation by amyloid-beta. *Nat Neurosci* **16**, 613-621 (2013).
4. Merlo, D., Mollinari, C., Racaniello, M., Garaci, E. & Cardinale, A. DNA Double Strand Breaks: A Common Theme in Neurodegenerative Diseases. *Curr Alzheimer Res* **13**, 1208-1218 (2016).
5. Mitra, J., *et al.* Motor neuron disease-associated loss of nuclear TDP-43 is linked to DNA double-strand break repair defects. *Proc Natl Acad Sci U S A* **116**, 4696-4705 (2019).
6. Provasek, V.E., Mitra, J., Malojirao, V.H. & Hegde, M.L. DNA Double-Strand Breaks as Pathogenic Lesions in Neurological Disorders. *Int J Mol Sci* **23**(2022).
7. Yu, X., Ji, C. & Shao, A. Neurovascular Unit Dysfunction and Neurodegenerative Disorders. *Front Neurosci* **14**, 334 (2020).
8. Kwon, H.S. & Koh, S.H. Neuroinflammation in neurodegenerative disorders: the roles of microglia and astrocytes. *Transl Neurodegener* **9**, 42 (2020).
9. Guzman-Martinez, L., *et al.* Neuroinflammation as a Common Feature of Neurodegenerative Disorders. *Front Pharmacol* **10**, 1008 (2019).

10. Sweeney, M.D., Kisler, K., Montagne, A., Toga, A.W. & Zlokovic, B.V. The role of brain vasculature in neurodegenerative disorders. *Nat Neurosci* **21**, 1318-1331 (2018).
11. Chomiak, A.A., *et al.* Nde1 is required for heterochromatin compaction and stability in neocortical neurons. *iScience* **25**, 104354 (2022).
12. Brown, R.E. & Freudenreich, C.H. Structure-forming repeats and their impact on genome stability. *Curr Opin Genet Dev* **67**, 41-51 (2021).
13. Guo, Y., *et al.* Histone H2A ubiquitination resulting from Brap loss of function connects multiple aging hallmarks and accelerates neurodegeneration. *iScience* **25**, 104519 (2022).
14. Hayflick, L. The Limited in Vitro Lifetime of Human Diploid Cell Strains. *Exp Cell Res* **37**, 614-636 (1965).
15. Hernandez-Segura, A., Nehme, J. & Demaria, M. Hallmarks of Cellular Senescence. *Trends Cell Biol* **28**, 436-453 (2018).
16. Kuilman, T., Michaloglou, C., Mooi, W.J. & Peeper, D.S. The essence of senescence. *Genes Dev* **24**, 2463-2479 (2010).
17. McHugh, D. & Gil, J. Senescence and aging: Causes, consequences, and therapeutic avenues. *J Cell Biol* **217**, 65-77 (2018).
18. Munoz-Espin, D. & Serrano, M. Cellular senescence: from physiology to pathology. *Nat Rev Mol Cell Biol* **15**, 482-496 (2014).
19. Sapieha, P. & Mallette, F.A. Cellular Senescence in Postmitotic Cells: Beyond Growth Arrest. *Trends Cell Biol* **28**, 595-607 (2018).
20. von Zglinicki, T., Wan, T. & Miwa, S. Senescence in Post-Mitotic Cells: A Driver of Aging? *Antioxid Redox Signal* **34**, 308-323 (2021).
21. Coppe, J.P., Desprez, P.Y., Krtolica, A. & Campisi, J. The senescence-associated secretory phenotype: the dark side of tumor suppression. *Annu Rev Pathol* **5**, 99-118 (2010).
22. Freund, A., Orjalo, A.V., Desprez, P.Y. & Campisi, J. Inflammatory networks during cellular senescence: causes and consequences. *Trends Mol Med* **16**, 238-246 (2010).
23. Wiley, C.D. & Campisi, J. The metabolic roots of senescence: mechanisms and opportunities for intervention. *Nat Metab* **3**, 1290-1301 (2021).
24. Lasry, A. & Ben-Neriah, Y. Senescence-associated inflammatory responses: aging and cancer perspectives. *Trends Immunol* **36**, 217-228 (2015).
25. Kuilman, T. & Peeper, D.S. Senescence-messaging secretome: SMS-ing cellular stress. *Nat Rev Cancer* **9**, 81-94 (2009).
26. Birch, J. & Gil, J. Senescence and the SASP: many therapeutic avenues. *Genes Dev* **34**, 1565-1576 (2020).
27. Gorski, J.A., *et al.* Cortical excitatory neurons and glia, but not GABAergic neurons, are produced in the Emx1-expressing lineage. *J Neurosci* **22**, 6309-6314 (2002).
28. Dewachter, I., *et al.* Neuronal deficiency of presenilin 1 inhibits amyloid plaque formation and corrects hippocampal long-term potentiation but not a cognitive defect of amyloid precursor protein [V717I] transgenic mice. *J Neurosci* **22**, 3445-3453 (2002).
29. Tsien, J.Z., *et al.* Subregion- and cell type-restricted gene knockout in mouse brain. *Cell* **87**, 1317-1326 (1996).
30. Kisanuki, Y.Y., *et al.* Tie2-Cre transgenic mice: a new model for endothelial cell-lineage analysis in vivo. *Dev Biol* **230**, 230-242 (2001).

31. Vaughan, D.E., Rai, R., Khan, S.S., Eren, M. & Ghosh, A.K. Plasminogen Activator Inhibitor-1 Is a Marker and a Mediator of Senescence. *Arterioscler Thromb Vasc Biol* **37**, 1446-1452 (2017).
32. Ozcan, S., *et al.* Unbiased analysis of senescence associated secretory phenotype (SASP) to identify common components following different genotoxic stresses. *Aging (Albany NY)* **8**, 1316-1329 (2016).
33. Tchkonia, T., Zhu, Y., van Deursen, J., Campisi, J. & Kirkland, J.L. Cellular senescence and the senescent secretory phenotype: therapeutic opportunities. *J Clin Invest* **123**, 966-972 (2013).
34. Singh, S., Saleem, S. & Reed, G.L. Alpha2-Antiplasmin: The Devil You Don't Know in Cerebrovascular and Cardiovascular Disease. *Front Cardiovasc Med* **7**, 608899 (2020).
35. Su, E.J. & Lawrence, D.A. alpha2 Antiplasmin and microvascular thrombosis in ischemic stroke. *Arterioscler Thromb Vasc Biol* **34**, 2522-2523 (2014).
36. Carpenter, S.L. & Mathew, P. Alpha2-antiplasmin and its deficiency: fibrinolysis out of balance. *Haemophilia* **14**, 1250-1254 (2008).
37. Shahidi, M. Thrombosis and von Willebrand Factor. *Adv Exp Med Biol* **906**, 285-306 (2017).
38. Kitamura, K., *et al.* Adrenomedullin: a novel hypotensive peptide isolated from human pheochromocytoma. *Biochem Biophys Res Commun* **192**, 553-560 (1993).
39. Kato, J., Tsuruda, T., Kita, T., Kitamura, K. & Eto, T. Adrenomedullin: a protective factor for blood vessels. *Arterioscler Thromb Vasc Biol* **25**, 2480-2487 (2005).
40. Sounni, N.E., Paye, A., Host, L. & Noel, A. MT-MMPS as Regulators of Vessel Stability Associated with Angiogenesis. *Front Pharmacol* **2**, 111 (2011).
41. Turner, R.J. & Sharp, F.R. Implications of MMP9 for Blood Brain Barrier Disruption and Hemorrhagic Transformation Following Ischemic Stroke. *Front Cell Neurosci* **10**, 56 (2016).
42. Boroujerdi, A., Welser-Alves, J.V. & Milner, R. Matrix metalloproteinase-9 mediates post-hypoxic vascular pruning of cerebral blood vessels by degrading laminin and claudin-5. *Angiogenesis* **18**, 255-264 (2015).
43. Lu, H., Cassis, L.A., Kooi, C.W. & Daugherty, A. Structure and functions of angiotensinogen. *Hypertens Res* **39**, 492-500 (2016).
44. Ameli, P.A., *et al.* Role of vasopressin and its antagonism in stroke related edema. *J Neurosci Res* **92**, 1091-1099 (2014).
45. Morton, J.J. & Padfield, P.L. Vasopressin and hypertension in man. *J Cardiovasc Pharmacol* **8 Suppl 7**, S101-106 (1986).
46. Ziv, I., *et al.* Increased plasma endothelin-1 in acute ischemic stroke. *Stroke* **23**, 1014-1016 (1992).
47. Alioglu, Z., *et al.* Increased plasma endothelin-1 levels in patients with intracerebral hemorrhage. *J Stroke Cerebrovasc Dis* **9**, 176-180 (2000).
48. Kohan, D.E., Rossi, N.F., Inscho, E.W. & Pollock, D.M. Regulation of blood pressure and salt homeostasis by endothelin. *Physiol Rev* **91**, 1-77 (2011).
49. Kolenc, O.I. & Quinn, K.P. Evaluating Cell Metabolism Through Autofluorescence Imaging of NAD(P)H and FAD. *Antioxid Redox Signal* **30**, 875-889 (2019).
50. DeSai, C. & Hays Shapshak, A. Cerebral Ischemia. in *StatPearls* (Treasure Island (FL), 2022).
51. Cheng L, B.D. *Essentials of Anatomic Pathology*, (Springer, 2016).

52. O'Brien, J.T. & Thomas, A. Vascular dementia. *Lancet* **386**, 1698-1706 (2015).
53. Bir, S.C., Khan, M.W., Javalkar, V., Toledo, E.G. & Kelley, R.E. Emerging Concepts in Vascular Dementia: A Review. *J Stroke Cerebrovasc Dis* **30**, 105864 (2021).
54. Wolters, F.J. & Ikram, M.A. Epidemiology of Vascular Dementia. *Arterioscler Thromb Vasc Biol* **39**, 1542-1549 (2019).
55. Kaplan, L., Chow, B.W. & Gu, C. Neuronal regulation of the blood-brain barrier and neurovascular coupling. *Nat Rev Neurosci* **21**, 416-432 (2020).
56. Iadecola, C. The Neurovascular Unit Coming of Age: A Journey through Neurovascular Coupling in Health and Disease. *Neuron* **96**, 17-42 (2017).
57. Admasu, T.D., Rae, M. & Stolzing, A. Dissecting primary and secondary senescence to enable new senotherapeutic strategies. *Ageing Res Rev* **70**, 101412 (2021).
58. Huang, W., Hickson, L.J., Eirin, A., Kirkland, J.L. & Lerman, L.O. Cellular senescence: the good, the bad and the unknown. *Nat Rev Nephrol* **18**, 611-627 (2022).
59. He, S. & Sharpless, N.E. Senescence in Health and Disease. *Cell* **169**, 1000-1011 (2017).
60. Paramos-de-Carvalho, D., Jacinto, A. & Saude, L. The right time for senescence. *Elife* **10**(2021).
61. Lodato, M.A., *et al.* Somatic mutation in single human neurons tracks developmental and transcriptional history. *Science* **350**, 94-98 (2015).
62. Lanctot, A.A., Peng, C.Y., Pawlisz, A.S., Joksimovic, M. & Feng, Y. Spatially dependent dynamic MAPK modulation by the Nde1-Lis1-Brap complex patterns mammalian CNS. *Dev Cell* **25**, 241-255 (2013).
63. Lanctot, A.A., *et al.* Loss of Brap Results in Premature G1/S Phase Transition and Impeded Neural Progenitor Differentiation. *Cell Rep* **20**, 1148-1160 (2017).

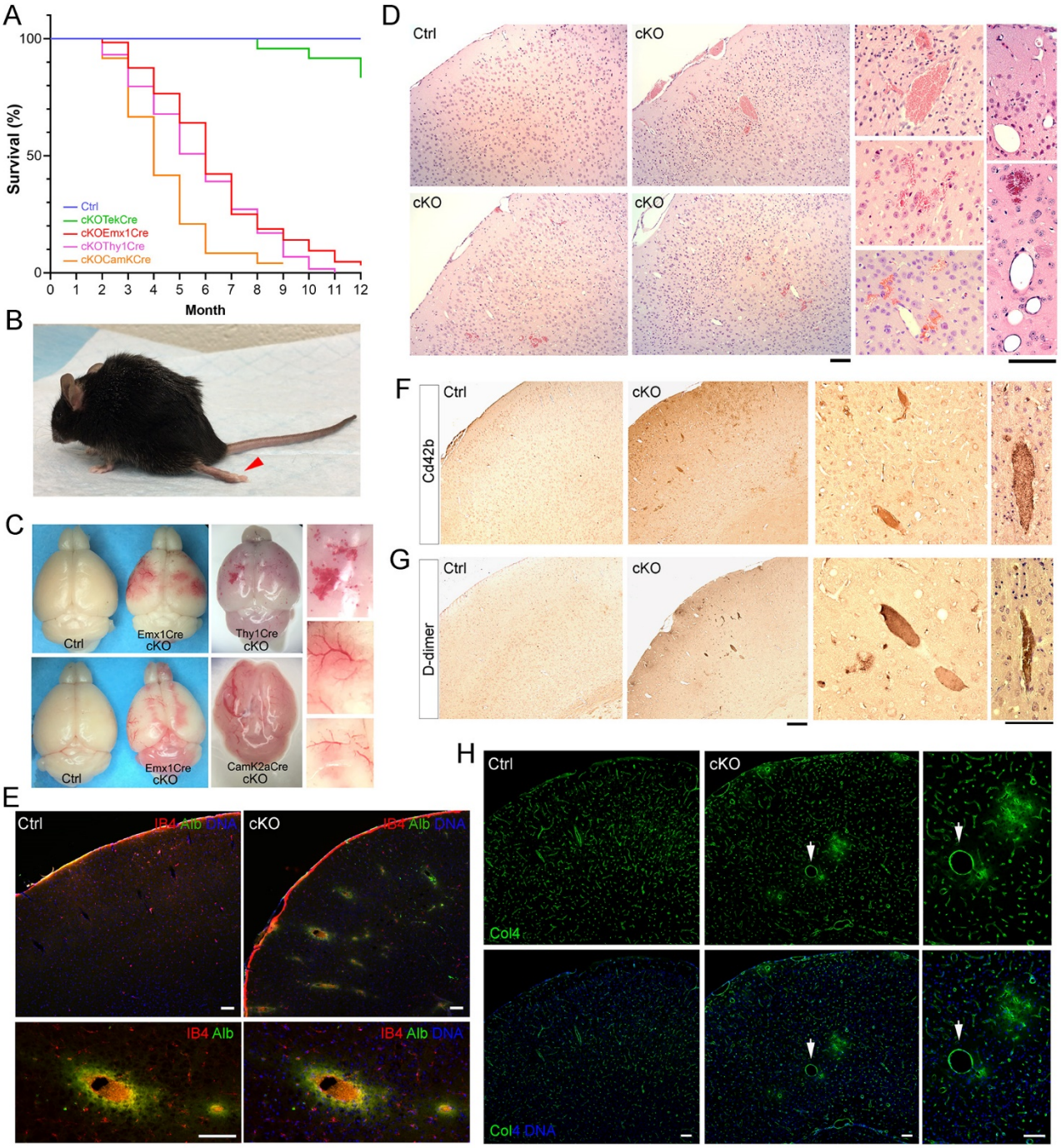
A
Survival (%)
100
50
0
0 1 2 3 4 5 6 7 8 9 10 11 12
Month
Ctrl
cKOTekCre
cKOEmx1Cre
cKOThy1Cre
cKOCamKCre
B
C
Ctrl
Emx1Cre cKO
Thy1Cre cKO
Ctrl
Emx1Cre cKO
CamK2aCre cKO
D
Ctrl
cKO
cKO
cKO
F
Cd42b
Ctrl
cKO
G
D-dimer
Ctrl
cKO
E
Ctrl
IB4 Alb DNA
cKO
IB4 Alb DNA
IB4 Alb
IB4 Alb DNA
H
Ctrl
cKO
Col4
Col4 DNA

Figure 1. Brap loss of function in cortical neurons results in midlife mortality and diverse cerebrovascular lesions.

(A) Kaplan Meier curves of mice with Brap conditional knockout in vascular endothelial cells (Tek-Cre, n=24), dorsal telencephalon neural progenitor cells (Emx1Cre, n=65), postnatal cortical and hippocampal neurons (Thy1Cre, n=60), excitatory neurons (Camk2aCre, n=25), and their control counterparts (n=47).

(B) A neural $Brap^{cKO}$ mouse that showed sudden paralysis of a hindlimb (monoplegia). The arrow indicates the dragging hindlimb. See also supplemental video.

(C) Representative brain images of neural $Brap^{cKO}$ mice that exhibited subarachnoid hemorrhage.

(D) H&E histology images show diverse cerebrovascular lesions, including subarachnoid and intracerebral hemorrhage, as well as aneurysm and occlusion of cerebral blood vessels in neural $Brap^{cKO}$ mice.

(E) Fluorescence immunohistological images of cortical sections double stained by Isolectin 4 (IB4, in red) and an albumin antibody (Alb, in green). Note the co-existence of cerebral vascular blockage and albumin extravasation in neural $Brap^{cKO}$ mice. Nuclear DNA was stained with Hoechst 33342.

(F&G) Representative immunohistochemistry images of cortical sections stained by antibodies against Cd42b or D-dimer.

(H) Representative fluorescence immunohistological images of cortical sections stained by an antibody to collagen IV (Col4, in green). The arrow indicates a bulging cerebral blood vessel in neural $Brap^{cKO}$ mice. Nuclear DNA was stained with Hoechst 33342.

Bars: 100 um.

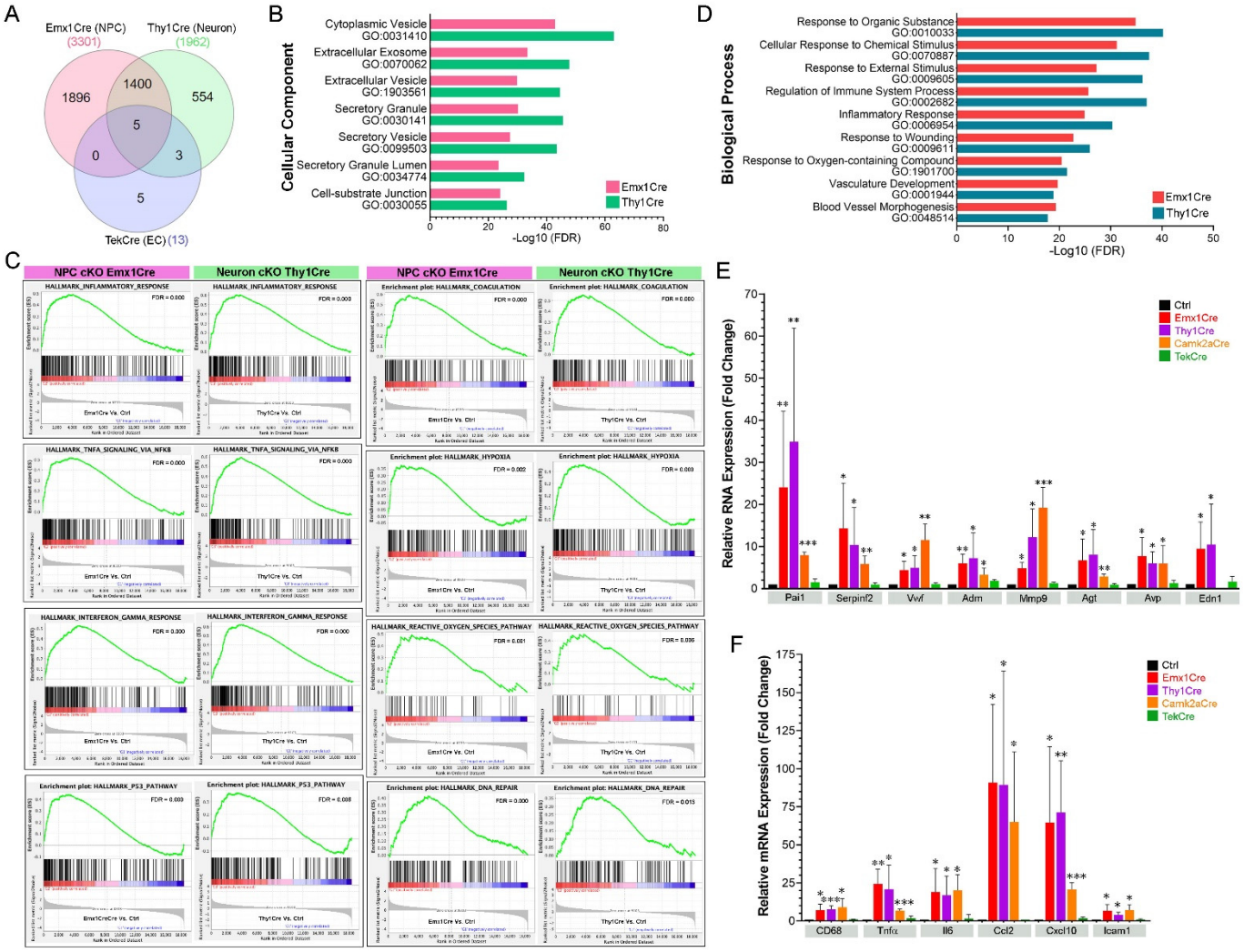
A
Emx1Cre (NPC)
(3301)
Thy1Cre (Neuron)
(1962)
1896
1400
554
5
0
3
5
TekCre (EC) (13)
B
Cellular Component
Cytoplasmic Vesicle
GO:0031410
Extracellular Exosome
GO:0070062
Extracellular Vesicle
GO:1903561
Secretory Granule
GO:0030141
Secretory Vesicle
GO:0099503
Secretory Granule Lumen
GO:0034774
Cell-substrate Junction
GO:0030055
Emx1Cre
Thy1Cre
-Log10 (FDR)
D
Biological Process
Response to Organic Substance
GO:0010033
Cellular Response to Chemical Stimulus
GO:0070887
Response to External Stimulus
GO:0009605
Regulation of Immune System Process
GO:0002682
Inflammatory Response
GO:0006954
Response to Wounding
GO:0009611
Response to Oxygen-containing Compound
GO:1901700
Vasculature Development
GO:0001944
Blood Vessel Morphogenesis
GO:0048514
Emx1Cre
Thy1Cre
-Log10 (FDR)
C
NPC cKO Emx1Cre
Neuron cKO Thy1Cre
HALLMARK_INFLAMMATORY_RESPONSE
HALLMARK_TNFA_SIGNALING_VIA_NFKB
HALLMARK_INTERFERON_GAMMA_RESPONSE
Enrichment plot: HALLMARK_P53_PATHWAY
Enrichment plot: HALLMARK_COAGULATION
Enrichment plot: HALLMARK_HYPOXIA
HALLMARK_REACTIVE_OXYGEN_SPECIES_PATHWAY
Enrichment plot: HALLMARK_DNA_REPAIR
E
Relative RNA Expression (Fold Change)
Ctrl
Emx1Cre
Thy1Cre
Camk2aCre
TekCre
Pai1
Serpinf2
Vwf
Adm
Mmp9
Agt
Avp
Edn1
F
Relative mRNA Expression (Fold Change)
Ctrl
Emx1Cre
Thy1Cre
Camk2aCre
TekCre
CD68
Tnfα
Il6
Ccl2
Cxcl10
Icam1

Figure 2. Significant upregulation of genes mediating cell secretion, inflammation, vascular changes, and DNA damage repair in cortical tissues of neural Brap^{cKO} mice.

(A) Venn diagram of significantly upregulated genes in cerebral cortices of mice with Brap conditional knockout in vascular endothelial cells (Tek-Cre, n=5), dorsal telencephalon neural progenitor cells (Emx1Cre, n= 6), or postnatal cortical and hippocampal neurons (Thy1Cre, n=5) at 3-4 months of age relative to age-matched control mice (n=4).

(B) Gene Ontology Cellular Component terms identified in significantly upregulated cortical protein coding genes of mice with Brap conditional knockout in dorsal telencephalon neural progenitor cells (Emx1Cre), or postnatal cortical and hippocampal neurons (Thy1Cre). Shown are selected enrichment terms with FDR values.

(C) Selected GSEA of hallmark pathways enriched in unique cortical genes identified from mice with Brap conditional knockout in dorsal telencephalon neural progenitor cells (Emx1Cre), or postnatal cortical and hippocampal neurons (Thy1Cre). Shown are enrichment score plots with FDR values compared to cortical genes identified from control mice.

(D) Gene Ontology Biological Process terms identified in significantly upregulated cortical protein coding genes of mice with Brap conditional knockout in dorsal telencephalon neural progenitor cells (Emx1Cre), or postnatal cortical and hippocampal neurons (Thy1Cre).

(E) RT-qPCR analyses of selected vasoactive genes in the cortical tissue of mice with Brap conditional knockout by Emx1Cre, Thy1Cre, Camk2aCre, or Tek-Cre mice at 3 months of age. Shown are relative expressions compared to mRNAs in age-matched control mice. Error bars represent SD; *$p < 0.05$; ** $p< 0.01$; *** $p< 0.001$, by ANOVA tests.

(F) RT-qPCR analyses of selected inflammatory genes in the cortical tissue of mice with Brap conditional knockout by Emx1Cre, Thy1Cre, Camk2aCre, or Tek-Cre mice at 3 months of age. Shown are relative expressions compared to mRNAs in age-matched control mice. Error bars represent SD; *$p < 0.05$; ** $p< 0.01$; *** $p< 0.001$, by ANOVA tests.

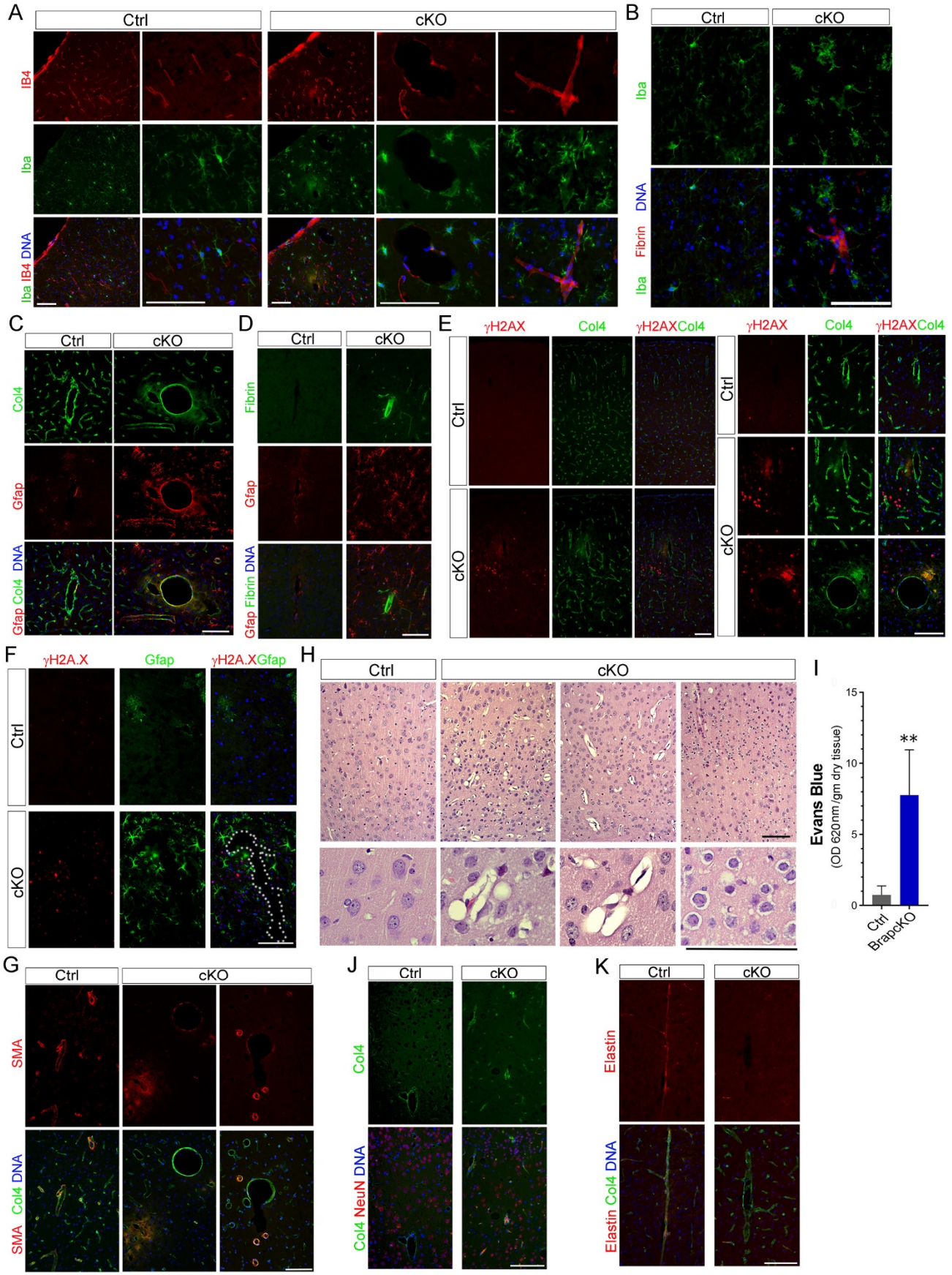
A
Ctrl
cKO
IB4
Iba
Iba IB4 DNA
B
Ctrl
cKO
Iba
DNA
Fibrin
Iba
C
Ctrl
cKO
Col4
Gfap
DNA
Gfap Col4
D
Ctrl
cKO
Fibrin
Gfap
DNA
Gfap Fibrin
E
γH2AX
Col4
γH2AXCol4
Ctrl
cKO
F
γH2A.X
Gfap
γH2A.XGfap
Ctrl
cKO
H
Ctrl
cKO
I
Evans Blue
(OD 620nm /gm dry tissue)
15
10
5
0
**
Ctrl
BrapcKO
G
Ctrl
cKO
SMA
SMA Col4 DNA
J
Ctrl
cKO
Col4
Col4 NeuN DNA
K
Ctrl
cKO
Elastin
Elastin Col4 DNA

Figure 3. Spatial correlation of DSBs with intertwined cerebral cortical glial activation and vascular lesions in neural BrapcKO mice

(A) Representative fluorescence immunohistological images of cortical sections stained by Isolectin 4 (IB4, in red) and the microglia marker Iba (in green). Note the enlarged microglia surrounding microbleeds and bulging cerebral blood vessels in neural $Brap^{cKO}$ mice.

(B) Representative fluorescence immunohistological images of cortical sections double stained by antibodies to fibrinogen (in red) and Iba (in green). Note the enlarged microglia next to a blood vessel with fibrin occlusion in the neural $Brap^{cKO}$ cortex.

(C) Representative fluorescence immunohistological images of cortical sections double stained by antibodies to Gfap (in red) and Col4 (in green). Note the reactive astrocytes with high Gfap surrounding a bulging cerebral blood vessel in the neural $Brap^{cKO}$ cortex.

(D) Representative fluorescence immunohistological images of cortical sections double stained by antibodies to Gfap (in red) and fibrin (in green). Note the strong Gfap in the region with vascular fibrin occlusion in the neural $Brap^{cKO}$ cortex.

(E) Representative fluorescence immunohistological images of cortical sections double stained by antibodies to the DSB marker γH2A.X and Col4, showing high abundance of γH2A.X signals nearby microbleeds and bulging blood vessels in the neural $Brap^{cKO}$ cortex.

(F) Representative fluorescence immunohistological images of cortical sections double stained by antibodies to the DSB marker γH2A.X (in red) and activated astrocytes Gfap (in green), showing the high abundance of both γH2A.X and Gfap signals in the vicinity of a misshapen blood vessel (marked by dotted outlines) in the neural $Brap^{cKO}$ cortex.

(G) Representative fluorescence immunohistological images of cortical sections double stained by antibodies to smooth muscle actin (SMA, in red) and Col4 (in green), showing reduced SMA in the vascular wall of neural $Brap^{cKO}$ cortex.

(H) H&E histology images show cerebral edema and enlarged perivascular space in neural $Brap^{cKO}$ mice.

(I) Evans blue assay reveals increased blood brain barrier permeability in pre-symptomatic $Brap^{cKONPC}$ mice. Error bars are SD. ** $p < 0.01$

(J&K) Representative fluorescence immunohistological images of cortical sections double stained by an antibody to Col4 (in green) and antibodies to NeuN or elastin (in red), showing the accumulation of Col4 with reduced elastin in the cerebral blood vessels of surviving neural $Brap^{cKO}$ mice.

Nuclear DNA was stained with Hoechst 33342 in blue. Bars: 100 um ~~or as indicated.~~

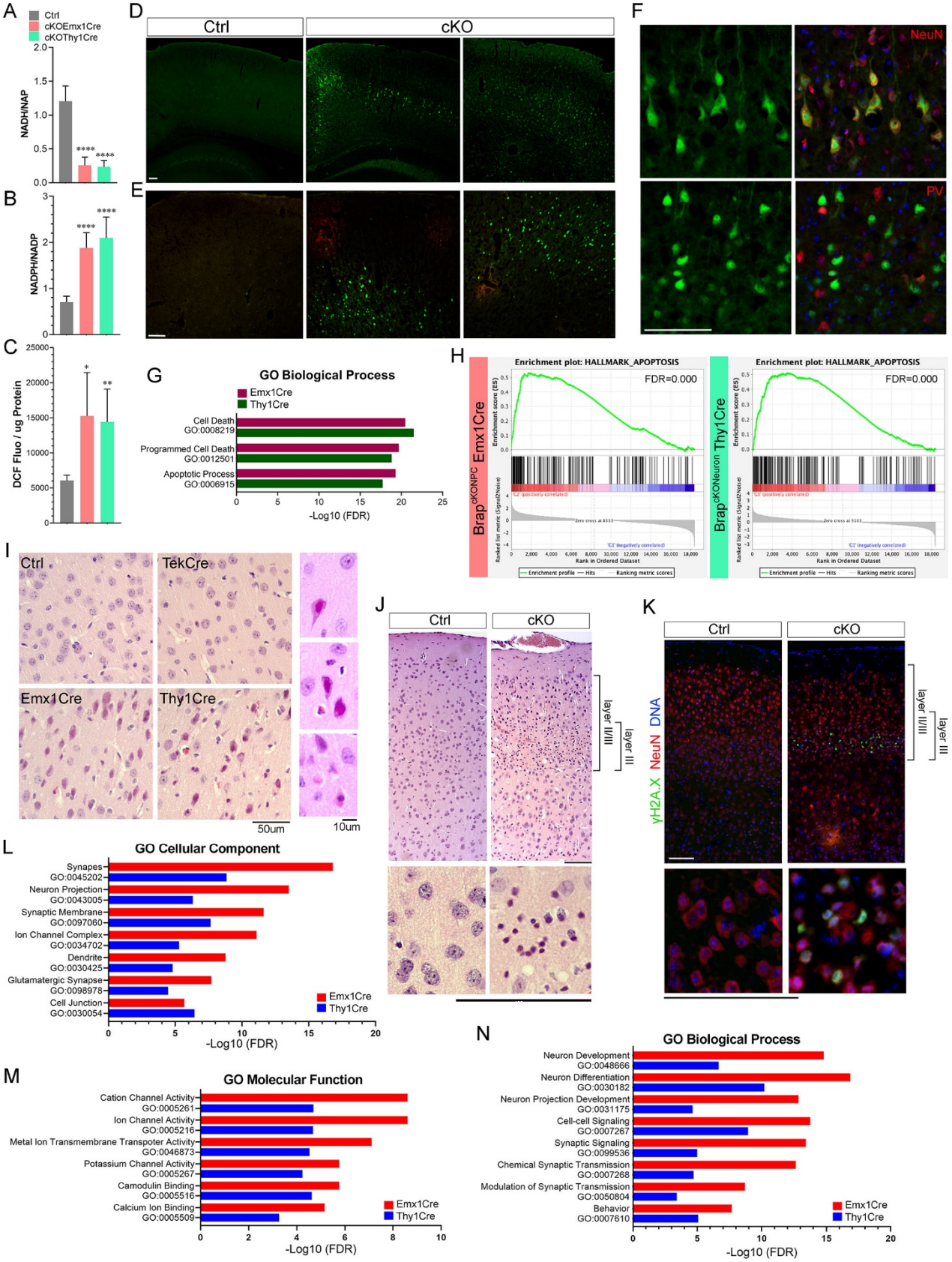
A
Ctrl
cKOEmx1Cre
cKOThy1Cre
NADH/NAP
B
NADPH/NADP
C
DCF Fluo / ug Protein
D
Ctrl
cKO
E
F
NeuN
PV
G
GO Biological Process
Emx1Cre
Thy1Cre
Cell Death
GO:0008219
Programmed Cell Death
GO:0012501
Apoptotic Process
GO:0006915
-Log10 (FDR)
H
Enrichment plot: HALLMARK_APOPTOSIS
FDR=0.000
Brap cKONPC Emx1Cre
Brap cKONeuron Thy1Cre
I
Ctrl
TekCre
Emx1Cre
Thy1Cre
50um
10um
J
Ctrl
cKO
layer II/III
layer III
K
Ctrl
cKO
DNA
NeuN
γH2A.X
layer II/III
layer III
L
GO Cellular Component
Synapes
GO:0045202
Neuron Projection
GO:0043005
Synaptic Membrane
GO:0097060
Ion Channel Complex
GO:0034702
Dendrite
GO:0030425
Glutamatergic Synapse
GO:0098978
Cell Junction
GO:0030054
Emx1Cre
Thy1Cre
-Log10 (FDR)
M
GO Molecular Function
Cation Channel Activity
GO:0005261
Ion Channel Activity
GO:0005216
Metal Ion Transmembrane Transpoter Activity
GO:0046873
Potassium Channel Activity
GO:0005267
Camodulin Binding
GO:0005516
Calcium Ion Binding
GO:0005509
Emx1Cre
Thy1Cre
-Log10 (FDR)
N
GO Biological Process
Neuron Development
GO:0048666
Neuron Differentiation
GO:0030182
Neuron Projection Development
GO:0031175
Cell-cell Signaling
GO:0007267
Synaptic Signaling
GO:0099536
Chemical Synaptic Transmission
GO:0007268
Modulation of Synaptic Transmission
GO:0050804
Behavior
GO:0007610
Emx1Cre
Thy1Cre
-Log10 (FDR)

Figure 4. Brain metabolic and neuronal dysfunction in neural BrapcKO mice.

(A-C) Relative levels of NADH (measured as NADH/NAD+ ratios), NADPH, (measured as NADPH/NAPD+ ratios), and ROS (measured as DCF fluorescence intensity /ug cortical protein) in cortical tissues of mice with Brap conditional knockout in dorsal telencephalon neural progenitor cells (Emx1Cre), postnatal cortical and hippocampal neurons (Thy1Cre), and Cre- controls. Error bars represent SD; *$p < 0.05$; ** $p< 0.01$; *** $p< 0.005$; **** $p< 0.0001$ by student's t-test.

(D&E) Representative images of autofluorescence of unstained cerebral cortical sections visualized by the green fluorescence channel (D) or both green and red fluorescence channels (E) by fluorescence microscopy.

(F) Immunohistological staining of cortical sections with neuronal markers NeuN or parvalbumin PV (both in red) reveals the overlap of green autofluorescent cells with NeuN immunoreactivity in the neocortex of $Brap^{cKONPC}$ mice. Nuclear DNA was stained with Hoechst 33342 in blue.

(G) Gene Ontology in Biological Process terms reveal the enrichments of cell death and apoptosis in upregulated DEGs from mice with Brap conditional knockout by Emx1Cre or Thy1Cre. Shown are selected enrichment terms with FDR values.

(H) GSEA of hallmark pathways reveals the association of apoptosis with unique cortical genes identified from mice with Brap conditional knockout by Emx1Cre or by Thy1Cre. Shown are enrichment score plots with FDR values compared to cortical genes identified from control mice.

(I&J) H&E histology images show cortical "red neurons" and "pseudo-laminar necrosis" in neocortical layer III of neural $Brap^{cKO}$ mice. The position of neocortical layer III is indicated.

(K) Representative fluorescence immunohistological images of cortical sections double stained by antibodies to cortical neurons (NeuN, in red) and the DSBs (γH2A.X, in green). Note the specific high levels of DSBs in layer III cortical neurons of neural $Brap^{cKO}$ mice. Nuclear DNA was stained with Hoechst 33342 in blue.

(L,M,N) Gene Ontology terms identified in significantly down regulated DEGs from cortical tissues of mice with Brap conditional knockout by Emx1Cre or Thy1Cre compared to control mice. Shown are selected enrichment terms in cellular component (L), molecular function (M), and biological process (N), respectively with FDR values.

Bars: 100 um or as indicated.